Indian Journal of Pure & Applied Physics
Vol. 60, July 2022, pp. 582-589

The Effectiveness of Ga Percent on the Electrical Characteristics of Al/CuIn$_{1-x}$Ga$_x$Se$_2$/ITO Schottky Junctions

S Hamrouni[a], Manea S AlKhalifah[b], K Ben Saad[a] & M S El-Bana[b,c*]

[a]Laboratoire de nanomatériaux et des systèmes pour les énergies renouvelables (LaNSER), Centre de Recherches et des Technologies de l'Energie (CRTEn), BP. 95, Hammam Lif 2050, Tunisia

[b]Materials Physics and Energy Laboratory, Department of Physics, College of Science and Arts at Ar Rass, Qassim University, ArRass 51921, Kingdom of Saudi Arabia

[c]Nanoscience & Semiconductor Laboratories, Department of Physics, Faculty of Education, Ain Shams University, Cairo, Egypt

Received 24 March 2022; accepted 17 June 2022

The electrodeposition method has been employed to deposit our quaternary semiconductor thin films CuIn$_{1-x}$Ga$_x$Se$_2$ (CIGS) which is deposited on Indium Tin Oxide (ITO) substrates with different Gallium ratios (x=0, 0.2, 0.4, 0.6, 0.8 and 1). The structural and optical characteristics variation of the films with altering Ga percent has been studied. The impact of changing the Ga/(In+Ga) atomic ratio on the electrical transport characteristics of electrodeposited CIGS thin films has been investigated using I-V and C-V measurements. All junctions have revealed the Schottky behavior. The energy gap of the studied compositions has increased with increasing Ga content. This lowered the values of charge mobility in the investigated films. Besides, the optimum Ga/(In+Ga) atomic proportion in the view of the obtained results is achieved by adding Ga with 20 %. Also, this finding approves the validation of our proposed criterion in expecting the most efficient photovoltaic junctions. The obtained results could improve our current knowledge of the quaternary photovoltaic solar cells.

Keywords: CIGS; Schottky junctions; Electrodeposition; Energetic factor; SCLC method

1 Introduction

The absorber layer is considered the solar cell heart as its properties affect the efficiencies of PV conversion. Thus, a great deal of attention has been driven to evolving inexpensive high-performance materials that could be a vital replacement for crystal silicon technology[1,2]. Therefore, ternary and quaternary chalcopyrite semiconductor thin films have attracted considerable interest for their high optical absorption coefficient (~10^5 cm^{-1}), direct band gap, long optoelectronic stability, and the possibility of preparing them using the low-cost techniques[2]. The most popular ternary chalcopyrite compounds are the $CuInSe_2$ (CIS) and $CuGaSe_2$ (CGS) which have 1.05 eV and 1.68 eV as energy gaps respectively[3-6]. While the quaternary $CuInGaSe_2$ (CIGS) owes an energy gap in the extent (1.04 - 1.68 eV) and it reveals conversion efficiencies up to 22.9%[1]. The CIGS composition has solved a weak point in the CIS material where CIS shows relatively low open-circuit voltage which results from its small band gap. The band gap of the CIGS material has varied based on the atomic ratio x=Ga/(In+Ga) percent. Controlling the CIGS band gap is a strong point in this material as its band gap can be tailored to correspond with the AM 1.5 solar spectrum[2,7,8]. Also, a clear effect has been noticed on the electrical and optoelectronic properties of this material according to the ratio x=Ga/(In+Ga). This comes out where this substitution changes the crystallographic parameters, a, b and c, and does not affect its spatial group which stills (I-42d). Furthermore, the crystallographic parameters of the elementary CIGS cell vary almost linearly between the CIS and the CGS cell's dimensions. This may be proved by the observed shift of the whole X-Ray spectrum of the samples with different Gallium percent[9-11].

Several techniques have been employed to deposit CIGS thin films such as sol-gel process[12,13], sputtering[14,15], chemical spray deposition[16,17], nano-particle precursor inks[18], electrochemical deposition[19,20], and others. Among these techniques, electrode position has been chosen as it is simple, economical, and considered a promising technique in high efficient low-cost solar cells[21]. In this context, the goal of this research is to examine the impact of

*Corresponding authors: (Email: mohammed.el-bana@bath.edu)

varying the Ga/(In+Ga) atomic proportion on the electrical transport characteristics of electrodeposited CIGS thin films using I-V and C-V measurements. Besides, determining the optimum Ga/(In+Ga) atomic percentage in the view of the obtained results and compare that with our proposed criterion in the text. The obtained results could improve our current knowledge on the quaternary photovoltaic solar cells.

2 Experimental preparation

The chemicals used in preparing our CIS, CGS and CIGS compositions have been provided from Sigma Aldrich with purities in the range of 99.99 %. For precise electrical measurements, Ossila's ITO glass substrates with six ITO fingers/cells (20Ω/square) have been utilized. Each finger has a dimension of $2.5 \times 3\ mm^2$ and a thickness of 100nm. The patterned substrates were cleaned using an ultrasonic bath at 60 °C for 10 min with distilled water, acetone, and isopropanol respectively, and then dried with Nitrogen gas after each step. The atomic ratio (x=Ga/Ga+In) in $CuIn_{1-x}Ga_xSe_2$ were varied. A stoichiometric aqueous solution have been prepared containing $CuCl_2$ (7mM), $InCl_3$ (0-5.7mM), $GaCl_3$ (0-5mM), SeO_2 (12mM) and 0.4 M of dehydrate tri-sodium citrate as mixing agent[19,22]. The solution pH has been adapted to be 1.8 by inserting a reasonable quantity of HCl. The electrode position was performed with a Potentiostat-Galvanostat, type Powerstat-05CE, with three cell electrodes consisting of a counter electrode (platinum plate), a working electrode (ITO substrate), and a reference electrode (Ag/AgCl). The Potentiostat-Galvanostat includes software that can control both the potential and the electric current across the cell. The working electrode potential was adjusted at the negative value -0.9V[21]. The deposition time was maintained at 20 min for all depositions. To enhance the film's crystallinity, samples have been annealed in an enclosed vacuum furnace. The annealing temperature has been increased in steps of 50 °C until reaching the recrystallization temperature of 350 °C[23] with keeping samples at each step for 10 min. Finally, samples were cooled slowly to room temperature. Top aluminum electrodes have been deposited through a special shadow mask using Edward Auto 306 Thermal Evaporator. The UV-Vis-NIR spectrometer was employed for the optical measurements. Keithley Semiconductor Characterization System SCS-4200 and the LCR Meter 4300 devices were utilized in the electrical measurements. The film thicknesses were estimated to be approximately 1μm for all samples using a profile meter (Filmetrics LS-DT2).

3 Results and discussion

3.1 Structural characterization

The XRD charts of the $CuIn_{1-x}Ga_xSe_2$ films are illustrated in Fig. 1. The CIGS thin films exhibited the polycrystalline phase and they reveal the tetragonal chalcopyrite structure as confirmed by comparing the obtained XRD patterns with the JCPDS (card number (35-1102)). The XRD patterns showed the main orientations such as (112), (220), and (116) that located at $2\theta = 26.68°, 45.37°,$ and $50.76°$ respectively for CIS/CIGS films. The (112) orientation is the one that presents the maximum probability of the appearance in the powder diagram. Also, other peaks have been observed which relate to conductive glass ITO substrate (JCPDS 06-0416). Based on the calculation of the orientation degree I_{hkl}/I_{112}, it is observed that the introduction of gallium favors the (220) and (116) orientations to the detriment of (112) orientation, see Table 1.

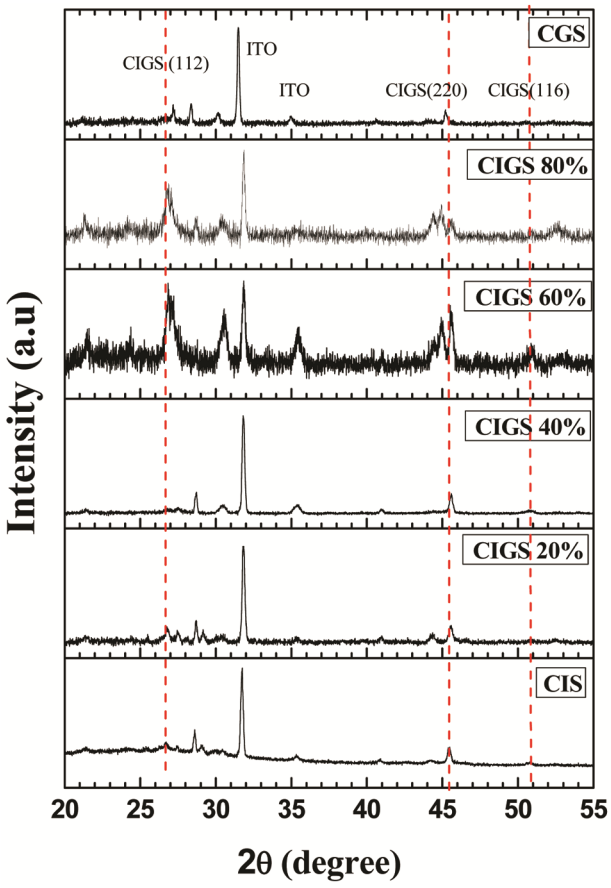

Fig. 1 — XRD charts of electrodeposited CIGS films at various Ga/(In+Ga) atomic ratios.

Table 1 — Calculation of the orientation degree I_{hkl}/I_{112} of CIGS films at various Ga/(In+Ga) atomic proportions.

I_{hkl}/I_{112}	CIS	CIGS 20%	CIGS 40%	CIGS 60%	CIGS 80%	CGS
$I_{(220)}/I_{(112)}$ (Experimental)	0.41	1.11	2.85	0.72	0.61	0.76
$I_{0(220)}/I_{0(112)}$ JCPDS (35-1102)	0.46	0.46	0.43	0.46	0.46	0.49
$I_{(116)}/I_{(112)}$ (Experimental)	0 .39	0.28	0.60	0.25	0.29	0.20
$I_{0(116)}/I_{0(112)}$ JCPDS (35-1102)	0.26	0.27	0.24	0.26	0.27	0.24

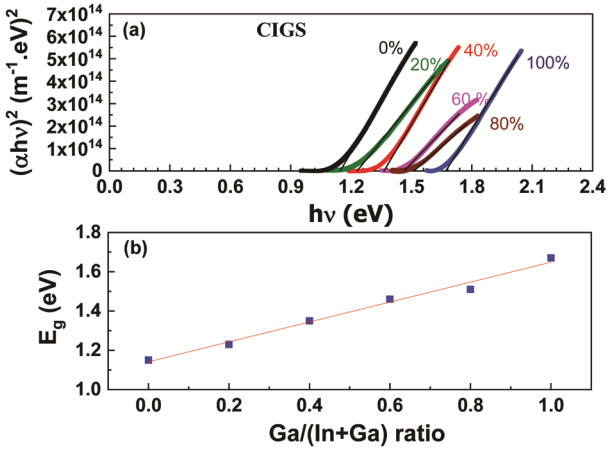

Fig. 2 — (a) Plots of $(\alpha h\nu)^2$ versus $h\nu$ for various compositions. (b) Variation of CIGS band gaps versus alteration in the Ga/(In + Ga) percentage.

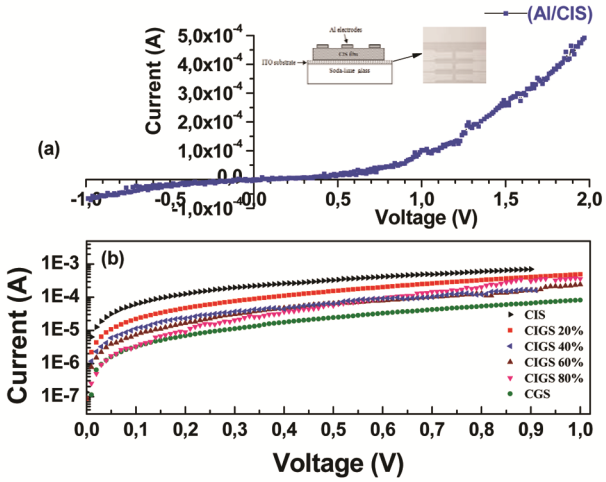

Fig. 3 — (a) Rectifying characteristics of Al/CIS contact. (b) The reliance of the forward I-V of Al/CIGS Schottky diode on the Ga percent.

Further, the characteristic XRD peaks revealed a significant shift to higher 2θ with the increase in Ga percent. This has been interpreted to the decrease in the lattice parameter of the chalcopyrite structure which results from replacing the relatively small Ga atoms at the expense of larger In atoms[24].

3.2 Optical features

The recorded reflection and transmission of CIGS films have been utilized to determine the film's absorption coefficient, α. Moreover, Tauc's equation has been used to evaluate both the type of optical transition and the films energy gap, E_g. The films have approved the following form of Tauc's law which presents the case of direct optical transition[25-27].

$$(\alpha h\nu)^2 = A(h\nu - E_g) \quad \ldots (1)$$

where A is a constant and $h\nu$ is the photon incident energy. This equation is applicable in the absorption zone (720-1200 nm) for CIS/CIGS films. In this range, the incident light whose energy is greater than the gap is absorbed. This absorption is ensured by the electrons of the valence band, which transit to the conduction band. Fig. 2(a) shows the extrapolation made for all films to estimate their energy gaps. The obtained energy gaps were expanded from 1.14 eV to 1.67 eV with rising the Ga percent as shown in Fig. 2(b). This finding has been expected due to the reduction of the dimension of the elementary CIGS's unit cell which results from replacing In atoms with the Ga ones.

3.3 Current-voltage analysis

The current-voltage (I-V) features' plot of Al/CIS contact in dark is shown in Fig. 3 (a) as a representative example of the I-V curves measured for all studied compositions. The I-V plot demonstrates that the Al contact is rectifying in nature like Shottky diodes. Fig. 3(b) explains the semi-logarithmic plot of I–V characteristics of Al/CIGS with varying the ratio x=Ga/(In+Ga). The obtained curves reveal a strong effect of varying the gallium percent on the manner of the Al/CIGS Schottky barrier diodes.

Following the thermionic emission model for similar diodes, the expression of the I-V characteristic is given by[28]:

$$I = I_s \exp\left[\frac{q(V-R_sI)}{nKT}\right]\left\{1 - \exp\left(\frac{q(V-R_sI)}{KT}\right)\right\} \quad \ldots (2)$$

where q is the charge carrier, n denotes the ideality factor, V is the applied voltage, K refers to the Boltzmann constant, R_s is the series resistance, and T

is the absolute temperature. Also, I_s denotes the pre-exponential factor (the saturation current): $I_s = A^* T^2 \exp\left[\frac{q\emptyset_b}{KT}\right]$, where $\emptyset_b$ is the Schottky barrier height at zero bias (at equilibrium), and A^* is the effective Richardson constant. With increasing the applied voltage to be greater than a few $\frac{KT}{q}$, the equation (2) can be further rewritten as[28]:

$$V = R_s I + n\emptyset_b - \frac{nKT}{q} \ln\left[\frac{I}{AA^*T^2}\right] \quad \ldots (3)$$

where A is the device's circular cross-section in diameter 1 μm. The slope of the expression (4) as a function of current is provided by:

$$\frac{dV}{d(\ln I)} = R_s I + \frac{nKT}{q} \quad \ldots (4)$$

The ideality factor (n) in the low applied voltage can be extracted from the formula:

$$n = \frac{q}{KT} \frac{dV}{d(\ln I)} \quad \ldots (5)$$

Figure 4(a) presents the alteration of $\frac{dV}{d(\ln I)}$ versus the current for all studied diodes. The values of the series resistance R_s have been determined from the slopes of the straight lines at high applied voltages. Also, the values of the ideality factor n for all diodes have been estimated by utilizing equation 6. Fig. 4(b) presents the dependence of both R_s&n on varying the ratio Ga/(In+Ga). It is noticed that both R_s & n increase with the increase in Ga percent in the investigated films. This can be referred to the increase in the percent of defects, grains, and diffusion of atoms in the composition with the increase in the ratio Ga/(In+Ga)[29]. The ideality factor values were found to be > 1. Despite the thermionic process is the main transport mechanism, the n values refer to a contribution of the recombination current. Therefore, the metal-insulator-semiconductor (MIS) configuration could be dominated rather than an ideal Schottky diode in the studied diodes[30].

Furthermore, the series resistance R_s as well as the barrier height $\emptyset_b$ have been investigated in response to variation of the Ga/(In+Ga) content. Cheung and Cheun method has been exploited in determining these parameters. This method follows the function[28].

$$H(I) = V - \frac{nKT}{q} \ln\left[\frac{I}{AA^*T^2}\right] \quad \ldots (6)$$

By considering the relation (3), the H(I) function can be reworded as:

$$H(I) = R_s I + n\,\emptyset_b \quad \ldots (7)$$

Figure 5(a) reveals the alteration of H(I) in response to the Ga/(In+Ga) percentage. The series resistance values have been determined from the slopes of the linear part of the curves. Whereas the y-axis intercepts have been used with knowing the n values to estimate the barrier height $\emptyset_b$.

It is noted that the above two methods have given almost the same values of the series resistance of the studied diodes. Also, it is seen that the diode barrier height $\emptyset_b$ lowers with increasing the Ga percent in the studied compositions (see Fig. 5 (b)). This trend could be interpreted to strengthen in energy difference $\Delta E_n = E_c - E_F$ with increasing the gallium percent in the investigated films in accordance with the formula[31]:

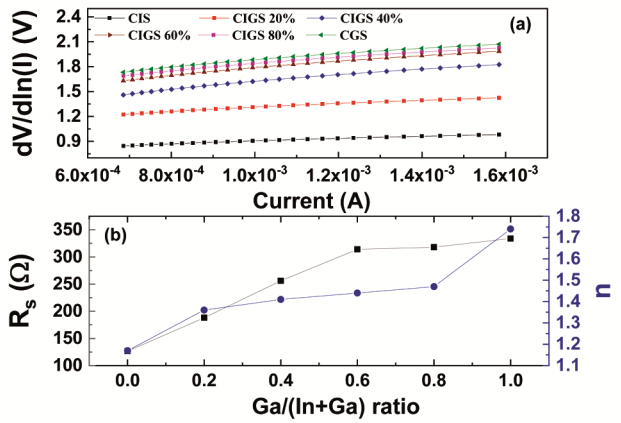

Fig. 4 — (a) The dV/dln(I) plots vs I for Al/CIGS Schottky diode. (b) Series resistance R_s and ideality factor n as a function of Ga/(In + Ga) percent for Al/CIGS Schottky diode.

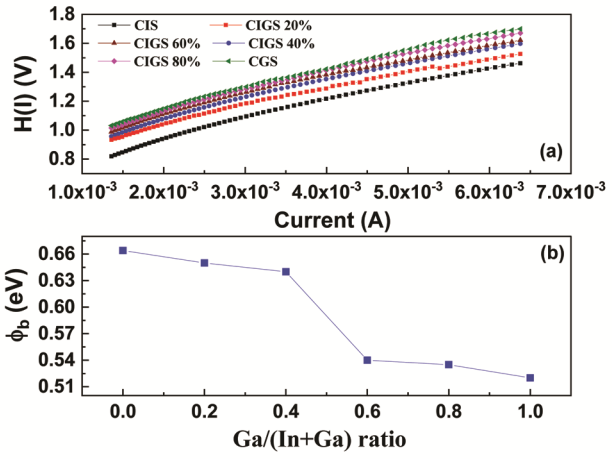

Fig. 5 — (a) Experimental H(I) that extracted from the I-V data for various Ga/(In + Ga) ratios. (b) Barrier height versus the variation in the Ga/(In+Ga) ratio for Al/CIGS Schottky diode.

$$\emptyset_b = V_{bi} + \frac{E_c - E_F}{q} = V_{bi} + \frac{KT}{q}\ln\frac{N_c}{N_A} \quad \ldots (8)$$

where V_{bi} is the semiconductor device's built-in potential, E_F denotes Fermi level energy, E_c refers to the conduction band energy, N_c is the effective density of states in the CIGS conduction band, and N_A is the concentration of carrier acceptors.

3.4 Capacitance-voltage measurements

The acceptors' concentration N_A in the electrodeposited films has been estimated from(C-V) measurements in the forward bias voltage at 100 kHz. The Mot - Schottky relation has been utilized in determining the acceptors' concentration N_A[32],

$$C^{-2} = \frac{2}{q\varepsilon_o\varepsilon_r N_A}[V_{bi} - V] \quad \ldots (9)$$

where V_0 the flat band, ε_r the semiconductor relative dielectric constant and ε_o the vacuum absolute dielectric constant. The N_A values have been evaluated from the straight lines' slopes exist in Fig. 6 (a) and with knowing the relative dielectric constant of a semiconductor ε_r(CIGS) =13.6[33].

Figure 6(b) implies the increase in the acceptors' concentration N_A with the increase in Ga percent in the investigated films (see Table 2). This behavior could be attributed to the possibility of changing the defect pair generation energy as a result of increasing the Ga percent[34]. Once the CIGS composition becomes non-stoichiometric, the major point defects that are usually generated are V_{Cu}, In_{Cu}, V_{Se}, and Cu_{In}. Also, the formation probability of Ga_{Cu} anti-site defect is more than the In_{Cu}[35]. Hence, boosting the Ga/(In+Ga) percentage within thin film reinforces the acceptor concentrations which were previously reduced by ionized V_{Cu}. This agrees well with the results in Fig. 6 (b).

Furthermore, each of the widths of the depletion region W_D, and the Debye screening distance L_D can be estimated using the following equations[31]:

$$W_D = \left(\frac{2\varepsilon_0\varepsilon_r}{qN_A}\right)^{1/2}\left(V - V_{bi} - \frac{KT}{q}\right) \quad \ldots (10)$$

$$L_D = \left(\frac{2\varepsilon_0\varepsilon_r}{q^2N_A}\right)^{1/2} \quad \ldots (11)$$

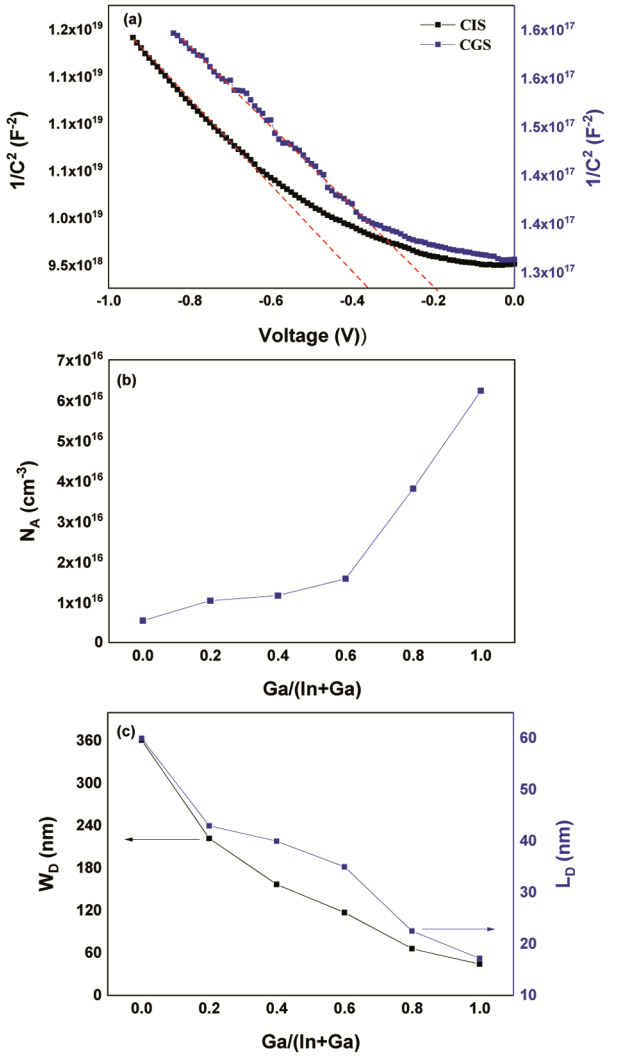

Fig. 6 — (a) Experimental C^{-2}-V characteristics of typical Al/CIS and Al/CGS Schottky diode as representative examples. (b) Variation of acceptor concentration N_A with Ga/(In+Ga) percent of Al/CIGS Schottky diode. (c) Variation of the Debye screening distance L_D and the depletion layer width W_D with Ga/Ga+In ratio in CIGS structure.

Table 2 — Some interesting electrical parameters that extracted from I-V and C–V analysis of the Al/CIGS Schottky diode in regards to varying the Ga percent

Ga (%)	R_s (Ω)	n	Φ_b (eV)	N_A (x 10^{16}cm^{-3})	W_D (nm)	L_D (nm)	μ x 10^{-4} (cm^2/VS)
0	126.5	1.17	0.66	0.54	361	60	3.55
20	188	1.36	0.65	1.03	222	43	3.46
40	256	1.41	0.64	1.16	157	40	2.93
60	314	1.44	0.54	1.58	117	35	2.54
80	318	1.47	0.53	3.80	65.9	22.5	1.28
100	334	1.74	0.52	6.23	44.3	17.2	0.89

Note that the depletion region is located at the interface of the diode on the semiconductor side.

The values of W_D are evaluated at V=0, see Table 2. Also, both parameters W_D and L_D have been decreased with the increase in Ga content in the investigated films (see Fig. 6 (c)).

3.5 Estimation of carrier mobility by the Space-Charge-Limited-Currents (SCLC) method

The carrier mobility in our junctions has been estimated by utilizing the (SCLC) method. The investigated junctions have revealed the characteristics that enable applying this mechanism. Where this mechanism is applicable in the case of ohmic conduction which appears when the current increases super linearly[36]. Fig. 7(a) implies the forward bias logarithmic I–V characteristic graph of Al/CIS Schottky junction as a representative example of our studied junctions. It is noted that there are two regions at voltages below 1.5V (region I) and at voltages above 1.5 V (region II). In region I, the rectifying conduction is dominant. While in region II, a linear behavior is seen which indicates the ohmic conduction. This behavior follows the characteristics of SCLC where $I \propto V$. Regards to this trend, the following expression has been used to determine carrier mobility.

$$J = N_A q \mu \frac{V}{d} \quad \ldots (12)$$

where J denotes the current density, V is the applied voltage, N_A is the acceptors' concentration, q is the electronic charge, μ is the mobility of charge carriers, and d is the thickness of the CIGS films. Fig. 7(b) displays the dependence of carrier mobility on the variation of Ga/(In+Ga) ratio. It is noted that the mobility reduces with boosting the Ga percent. This means that the extra increase in Ga percent in such a composition affects the performance of the diode.

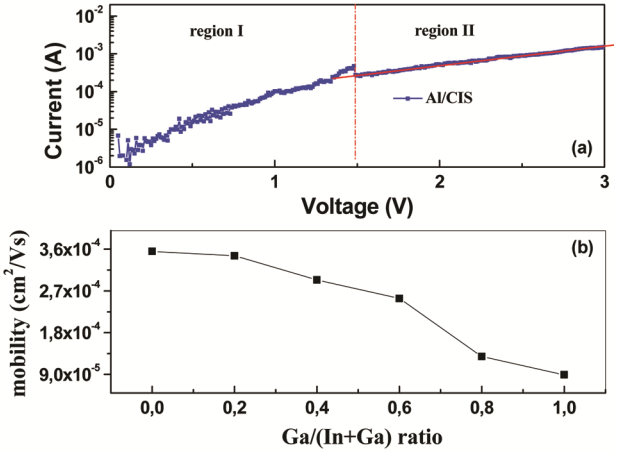

Fig. 7 — (a) I-V characteristics of Al/CIS Schottky junction. (b) Mobility of charge carriers in CIGS structure for different gallium ratios.

3.6 Prediction of junctions' efficiency

To examine the effect of increasing Ga percent on the Schottky junction efficiency, we have tried to use a criterion that could be applied to any other junctions. This criterion comes out from comparing three interesting parameters which are the ratio $\frac{E_g}{n}$, barrier heightΦ_b, and the energetic factor of the junctionE_{gg}($E_{gg} = \frac{E_g}{n} - \Phi_b$). Generally, to achieve a good photoelectric effect with these kinds of samples, it is necessary to reduce the thermoelectric effect corresponding to the dark current density to its minimum value. Also, in an ideal condition, the electric potential produced by a cell should be comparable to the absorber layer energy gap ($qV \approx E_g$). With regards to this condition, the transition of charges through the Schottky junction is possible. Therefore, the following expression can be used to estimate the junction current density:

$$J \approx J_{ph} - A^* T^2 \exp\left(\frac{E_{gg}}{kT}\right) \quad \ldots (13)$$

When E_{gg}has the lowest possible value, the exponential function reaches its minimum value which leads to increasing the current density to its highest value. This condition has been achieved in the case of 20% of Ga percent (cf., Fig. 8 (a)). This percent must be used to provide, in our conviction, the highest efficiency for the CIGS cells.

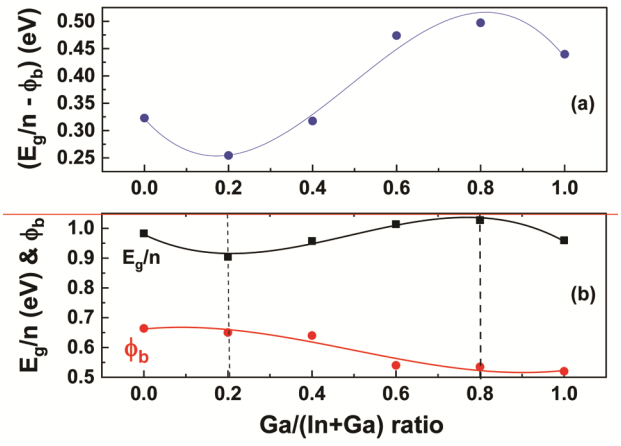

Fig. 8 — (a) Variation of $\left(\frac{E_g}{n} - \Phi_b\right)$ for different Gallium percent. (b) Comparison between Φ_b and $\frac{E_g}{n}$ ratio.

On the other hand, it is referred in several reports that the Schottky junction efficiency increases with increasing the barrier height. Also, Wei *et.al.*[35] have proposed that the best condition for photovoltaic Schottky junctions is achieved when the barrier heightΦ_b beless thanhalf of the gap ($E_g/2$). It is believed that this condition is not sufficient to judge the efficiency of the photovoltaic cell. Hence, we have modified their condition by dividing the energy gap by the ideality factor$n(E_g/n)$, and the higher efficiency could be achieved when the ratio $\frac{E_g}{n}$ becomes minimum and Φ_b becomes maximum as possible. Our suggestion is more logical in expecting the efficiency of the photovoltaic junctions where it enables us to check the efficiency of the junction from the trend of the three parameters $\frac{E_g}{n}$, Φ_b, and the energetic factor of the junction E_{gg}. Fig. 8(b) shows the variation of both $\frac{E_g}{n}$ and $\Phi_b$versus the Ga/(In + Ga) content. Again the Ga of 20% percent achieves the proposed condition where $\frac{E_g}{n}$ reaches its minimum value whereas Φ_b reaches its maximum value. This is inconsistence with the minimum value of E_{gg} seen in Fig. 8(a). These findings confirm two important issues in the current study. Firstly, the material with 20 % percent of Ga could be the best choice to be used as a good absorber layer in solar cells. Secondly, our criterion by utilizing the three parameters$\frac{E_g}{n}$, Φ_b, and $E_{gg}$to examine the effect of increasing Ga percent on the Schottky junction efficiency can be applied to other similar junctions in this field of research.

4 Conclusion

$CuIn_{1-x}Ga_xSe_2$ (CIGS) (x from 0 to 1 in steps of 0.2) films have been prepared using the electrodeposition technique. Schottky junctions have been fabricated by depositing these films on top of ITO substrates. Aluminum has been chosen to be the top electrode. Structural, electrical, and optical features have been investigated in regards to the variation in the Ga percent. The CIGS thin films exhibited the polycrystalline phase and revealed the tetragonal chalcopyrite structure. A noticeable drift in the characteristic peak (112) to higher 2θ with the increase in Ga content is observed. This has been interpreted to the decrease in the lattice parameter which results in the chalcopyrite structure due to replacing the larger In atoms with the relatively small Ga atoms. A blue shift in the energy gap to higher energy is noticed with the increase in Ga percent in the studied materials. The impact of varying the Ga/(In+Ga) atomic percentage on the electrical transport characteristics of CIGS thin films has been examined by using the I-V, and C-V analysis. All of the used junctions have exhibited Schottky behavior. An increase in each of the ideality factor n, the series resistance $R_{s,}$ and the carrier acceptors N_A of the CIGS films has been noticed with boosting the Ga/(In + Ga) ratio. Also, a decrease in each of the depletion layer width W_D and the Debye screening distance L_D has been noticed. By applying the SCLC mechanism in Al/CIGS Schottky diode, the mobility of the trapped carrier has been noted to decrease as well with raising the Ga percent. Besides, the optimum Ga/(In+Ga) atomic percentage in the view of the obtained results is achieved by adding Ga with 20 %. Although, the increase in Ga percent in the CIGS structures helps to increase the energy gap to be close to the optimum value needed in solar cells (1.5 eV). Other problems have been raised where the increase in Ga content could be associated with the increase in undesirable defects that might reduce the Debye length and consequently decrease the CIGS electric performances. This may be achieved by using the known vacuum deposition techniques that control the thickness of the thinnest films. In addition, our findings approve the validation of our proposed criterion in expecting the most efficient photovoltaic junctions. The obtained results could enhance our present knowledge of the quaternary photovoltaic solar cells.

References

1 Mandati S, Dey S R, Joshi S V & Sarada B V, *Sol Energy J*, 181 (2019) 396.
2 Mandati S, Sarada B V, Dey S R & Joshi S V, *Semiconductors*, (2018) 109.
3 Hamrouni S, AlKhalifah M S, Boujmil M & Saad K B, *Appl Surf Sci*, 292 (2014) 231.
4 Guillen C & Herrero J, *Sol Energy Mater Sol Cells* 43 (1996) 47.
5 Paorici C, Zanotti L, Romeo N, Sberveglieri G & Tarricone L, *Sol Energy Mater*, 1 (1979) 3.
6 Jackson P, Hariskos D, Wuerz R, Kiowski O, Bauer A, Friedlmeier T M & Powalla M, *Phys Status Solidi* (RRL)-*Rap Res Lett*, 9 (2015) 28.
7 Wei S H, Zhang S & Zunger A, *Appl Phys Lett*, 72 (1998) 3199.
8 Albin D, Tuttle J, Mooney G, Carapella J, Duda A, Mason A & Noufi R, *IEEE Conf on Photovolt Special*, (1990) 562.
9 Lee D Y, Park S & Kim J, *Curr Appl Phys*, 11 (2011) S88.
10 Mahendran C & Suriyanarayanan N, *Phys B: Condensed Matter*, 408 (2013) 62.

11 Kapur V K, Bansal A, Le P & Asensio O I, *Thin Solid Films*, 431 (2003) 53.
12 Faraj M, Ibrahim K & Salhin A, *Mater Sci Semicond Process*, 15 (2012) 206.
13 Luo P, Zhu C & Jiang G, *Solid State Commun*, 146 (2008) 57.
14 Ayyildiz E, Lu C N & Türüt A, *J Electron Mater*, 31 (2002) 119.
15 Calixto M E, Dobson K D, McCandless B E & Birkmire R W, *J Electrochem Soc*, 153 (2006) G521.
16 Bolotnikov A E, Boggs S E, Chen C H, Cook W R, Harrison F A & Schindler S M, Properties of Pt Schottky type contacts on high-resistivity CdZnTe detectors, *Nucl Instrum Meth Phys Res Sec A*, 482 (2002) 395.
17 Tung R, Mater Sci Eng, 35 (2001) 1.
18 Schlenker E, Mertens V, Parisi J, Reineke-Koch R & Köntges M, *Phys Lett A*, 362 (2007) 229.
19 Lee H, Lee W, Kim J Y, Ko M J, Kim K, Seo K, Lee D K & Kim H, *Electrochim Acta*, 87 (2013) 450.
20 Dharmadasa I, Bunning J, Samantilleke A & Shen T, *Sol Energy Mater Sol Cells*, 86 (2005) 373.
21 Londhe P U, Rohom A B, Fernandes R, Kothari D & Chaure N B, *ACS Sustain Chem Eng*, 6 (2018) 4987.
22 Kohara N, Nishiwaki S, Hashimoto Y, Negami T & Wada T, *Sol Energy Mater Sol Cells*, 67 (2001) 209.
23 Adel C, Fethi B M & Brahim B, *Appl Phys A*, 122 (2016) 62.
24 Shafarman W N, Klenk R & McCandless B E, *J Appl Phys*, 79 (1996) 7324.
25 Radaf I E, Al-Zahrani H, Fouad S & El-Bana M S, *Ceram Int J*, 46 (2020) 18778.
26 AlKhalifah M, Radaf I E & El-Bana M S, *J Alloys Compd*, 813 (2020) 152169.
27 El-Bana M S & Radaf I E, *Phys B: Condensed Matter*, (2022) 413705.
28 Hamrouni S, AlKhalifah M, El-Bana M S, Zobaidi S & Belgacem S, *Appl Phys A*, 124 (2018) 555.
29 Fiat S, Polat I, Bacaksiz E, Kompitsas M & Çankaya G, *Curr Appl Phys*, 13 (2013) 1112.
30 Chawanda A, Coelho S M, Auret F D, Mtangi W, Nyamhere C, Nel J M & Diale M, *J Alloys Compd*, 513 (2012) 44.
31 Cheung S & Cheung N, *Appl Phys Lett*, 49 (1986) 85.
32 Radaf I E & El-Bana M S, *Phys B: Condensed Matter*, 584 (2020) 412067.
33 Boubakeur M, Aissat A, Arbia M B, Maaref H & Vilcot J, *Superlatt Microstruct*, 138 (2020) 106377.
34 Zhang S, Wei S H, Zunger A, Katayama-Yoshida H, *Phys Rev B*, 57 (1998) 9642.
35 Wei S H & Zunger A, *J Appl Phys*, 78 (1995) 3846.
36 Visschere P D, Woestenborghs W & Neyts K, *Organic Electron*, 16 (2015) 212.